

## Article

# Influence of Combined Air-Entraining Superplasticizer and Surface Treatments on Airport Pavement Concrete against Salt Freezing

Molan Li <sup>1</sup>, Yong Lai <sup>2</sup>, Daoxun Ma <sup>3</sup>, Junjie Wang <sup>1,\*</sup> , Lei Xu <sup>1</sup>, Zhibin Gao <sup>4</sup>, Yan Liu <sup>2</sup>, Le Li <sup>1</sup>, Yaopu Guo <sup>1</sup>, Lifan Zheng <sup>1</sup> and Yi Zhang <sup>1</sup> 

<sup>1</sup> Department of Civil Engineering, Tsinghua University, Beijing 100084, China

<sup>2</sup> Beijing Super-Creative Technology Co., Ltd., Beijing 100621, China

<sup>3</sup> China Airport Construction Group Corporation of CACC, Beijing 100621, China

<sup>4</sup> Capital Airport Group Co., Ltd., Beijing 100621, China

\* Correspondence: junjiawang@tsinghua.edu.cn; Tel.: +86-(0)-178-37-238-638

**Abstract:** Effective improvement of the frost resistance of concrete in cold regions is critical for the durability of airport pavement concrete in plateau. This paper intends to contribute to a better knowledge of the effects of combined air-entraining superplasticizer and surface treatments on the resistance against freezing-thawing and salt freezing. First, an optimum mixing by considering w/c, cement content, sand ratio, and air-entraining superplasticizer was obtained by comparing compressive and flexural strength, microstructure, pore distribution, and resistance to freezing-thawing of different mixes. From the results, a concrete mix with air-entraining superplasticizer, w/c = 0.4, cement amount at 330 kg/m<sup>3</sup>, and sand ratio = 0.3 was selected for airport pavement. Then, this mix was subjected to salt freezing with different surface treatments (smoothing, brushing, spraying with silane, and impregnating with silane), and the spalled mass loss in salt freeze cycles was reported. The results show that combined use air-entraining superplasticizer and surface treatments can provide an obvious improvement on the resistance to salt freezing. Compared to silane impregnation, surface treatment by silane spraying performed much better in early time.

**Keywords:** freeze-thawing; salt-freezing; airport pavement; silane spraying and immersion; air-entraining superplasticizer



**Citation:** Li, M.; Lai, Y.; Ma, D.; Wang, J.; Xu, L.; Gao, Z.; Liu, Y.; Li, L.; Guo, Y.; Zheng, L.; et al. Influence of Combined Air-Entraining Superplasticizer and Surface Treatments on Airport Pavement Concrete against Salt Freezing. *Coatings* **2023**, *13*, 372. <https://doi.org/10.3390/coatings13020372>

Academic Editors: Valeria Vignali and Giorgos Skordaris

Received: 29 November 2022

Revised: 23 December 2022

Accepted: 3 February 2023

Published: 6 February 2023



**Copyright:** © 2023 by the authors. Licensee MDPI, Basel, Switzerland. This article is an open access article distributed under the terms and conditions of the Creative Commons Attribution (CC BY) license (<https://creativecommons.org/licenses/by/4.0/>).

## 1. Introduction

As one of the construction materials currently being used in large quantities [1], concrete is becoming more demanding in terms of its performance as the range of applications expands [2–4]. Unique environments put forward special requirements, such as in the highlands: high altitude, thin air, and low air pressure [5]. Concrete used on the plateau is subject to significant temperature variations [6], precipitation, snowfall, de-icing fluids, and snowmelt, among which the most damaging one is freeze-thawing erosion. Repeated freeze-thaw cycles can lead to cracking and spalling of concrete, which can lead to structural damage [7] and fail to meet the durability requirements of the application. Wu et al. [7] added cellulose/polyvinyl alcohol hydrogel in concrete to block crack expansion and reported an improvement in the freeze-thaw resistance of concrete. Zhang et al. [8] found that adding a small amount of nano-silica into concrete can reduce the chloride ion diffusion coefficient and improve the freeze-thaw resistance of concrete. Şahin et al. [9] pointed out that different freezing methods significantly impact the evaluation of freeze-thaw resistance of concrete mixtures, such as freezing rate, temperature duration, etc.

The two most classical theories about freeze-thaw damage are hydrostatic pressure theory [10] and osmotic pressure theory [11]. In short, water in pores freezes into ice in concrete, and cracks occur and gradually expand in concrete due to pressure on pore walls

caused by volume expansion or osmotic pressure. Many factors affect the frost resistance of concrete, such as salt solution types and concentration, freezing temperature, water-cement ratio, air-entrainment, admixtures, concrete surface microscopic state, aggregates, etc. Among them, the degree of water saturation and pore structure [12] of concrete are the main factors. The concrete with a higher porosity but a similar strength usually has a better frost resistance [13]. Water saturation and pore structure of materials mainly depend on water-cement ratio and admixture [14–17], etc.

The water-cement ratio in concrete is positively proportional to the amount of porosity at the cement interface, and also has a significant effect on the compressive strength of the material [18]. Microcracks during freeze-thaw cycles develop along with the porous interface between the cement paste and fine aggregates, and reduction of the water-cement ratio can effectively reduce the number of interfacial pores, which effectively improves the frost resistance of cementitious materials.

Research reported that the addition of superplasticizer to concrete can enhance substantial water reduction, and the addition of air-entraining agents can improve the frost resistance of concrete [10,19]. Adding the suitable admixtures can effectively enhance the performance of concrete, significantly reduce the surface tension of concrete [20], improve the concrete's compatibility, reduce water secretion and segregation, improve the frost resistance and durability of concrete, etc., so that concrete can be highly durable in a high plateau environment.

When sand-aggregate ratio in concrete increases, the specific surface area and water requirement of sand increase accordingly. Under the same sand fineness modulus conditions, the strength of concrete at 28 days decreases with the increase in sand-aggregate ratio. Therefore, a reasonable sand-aggregate ratio admixture should be determined through tests. The optimum amount of sand-aggregate ratio can reduce the void ratio of concrete and improve the long-term performance and durability of concrete [21].

Concrete surface treatment can effectively protect the concrete, especially in extremely cold conditions [22]. The surface of an airport roadway has a critical impact on the safety of aircraft operations. Surface treatment is a very effective way to reduce the deterioration of concrete structures in extreme environments and to extend the life of the roadway effectively [23]. Alkyl alkoxysilane materials (silanes for short) are silicone materials that are commonly used for concrete surface treatment. When the silane is painted on the concrete surface, it will gradually penetrate the material and react with water under alkaline conditions inside the concrete to produce highly reactive hydroxylases, which will react with the hydroxyl groups on the concrete surface to produce a water-repellent net-like molecular structure [24] and adhere to the concrete surface, a process known as silane impregnation treatment [25]. Concrete impregnated with silane can make the internal structure water-repellent and isolate the penetration of external water-soluble aggressive media [26]. Basheer et al. [27] showed that the freeze-thaw resistance of concrete treated with silane impregnation was double that of untreated concrete. Silane impregnation is now commonly used in engineering for the durability and protection of service concrete.

This paper tries through seven groups of concrete samples with different cement proportions, air-entrained superplasticizers, water-cement ratios, and sand-aggregate ratios to investigate the effect of these variables on physical properties. The physical properties include compressive and flexural strength, microstructure and pore distribution, the relationship between freeze-thaw cycles and mass loss rate, and spalled mass loss in salt freeze cycles. Different surface treatments were applied on the surface of selected concrete samples subjected to salt freezing to explore the most suitable surface protection methods for airport pavement on a high plateau. The main novelty of this work is the combination of different surface treatment methods and the air-entraining superplasticizer for the concrete resistance of salt freezing.

## 2. Materials and Methods

### 2.1. Materials

PO 42.5 ordinary Portland cement conforming to Chinese national standard GB175-2007 [28] was used in this experiment. The content and physical properties of cement are given in Tables 1 and 2.

**Table 1.** Components and specific surface area of cement.

CaO	SiO <sub>2</sub>	Fe <sub>2</sub> O <sub>3</sub>	Al <sub>2</sub> O <sub>3</sub>	SO <sub>3</sub>	MgO	Chloride Ion	Natural Gypsum	Specific Surface Area
63%–67%	22%–24%	5%–7%	4%–6%	2.44%	1.58%	0.01%	4.50%	335 m <sup>2</sup> /kg

**Table 2.** Cement physical properties.

Initial Setting Times	Final Setting Times	3 Days Flexural Strength	3 Days Compressive Strength	28 Days Flexural Strength	28 Days Compressive Strength
180 min	235 min	4.9 MPa	22.5 MPa	8.6 MPa	48.3 MPa

Naphthalene ZH-3 air-entraining superplasticizer following the provisions of GB8076-2008 [29] was used. In order to determine the performance of this naphthalene-based air-entraining superplasticizer in practice, a series of experiments were conducted, as in Figure 1. The technical performance and experimental results of naphthalene ZH-3 air-entraining superplasticizer are listed in Tables 3 and 4.



**Figure 1.** Testing of flow diameter.

**Table 3.** Technical performance of naphthalene ZH-3 air-entraining superplasticizer.

Tests		Results
Water reduction rate (%)		19
Water secretion rate (%)		0
Air content (%)		3.5
Difference in coagulation time (min)	First condensation	25
	Final condensation	40

**Table 4.** Experimental results of naphthalene ZH-3 air-entraining superplasticizer.

Tests		Results
Compressive strength ratio (%)	3 days	140
	7 days	135
	28 days	119
Bending to tensile strength ratio (%)	28 days	114
Shrinkage ratio (%)	28 days	97

The test specimens were made in the laboratory following MH 5006-2015 [30] using a forced mixer to mix the concrete mixture to ensure the homogeneity of the concrete. Before mixing the concrete, the mixer was wetted and mixer plates to ensure that the water-cement ratio of each specimen is consistent with the design water-cement ratio.

The mixing procedure for concrete in this study is as follows: First the stone, cement, and sand were added into the mixer in turn and mixed for 120 s. Then, the mixture of superplasticizer and water were added to the mixer and mixed for 120 s before casting into the molds according to GBT 50081-2019 [31]. Then, test blocks were placed on a vibrating table for vibration. After 10 s of vibration, the cast surface was smoothed and covered with thick plastic sheets, and the specimens were water-cured (20 °C) after molding for 24 h.

By considering different cement amounts and adding air-entraining superplasticizer, water-cement ratios, and sand-aggregate ratios, mixing information in this study is shown in Table 5. The coarse aggregates consist of 16–31.5 mm big stones and 4.75–16 mm small stones, and the sieving curves for the two types of aggregates are shown in Figure 2a. The fine aggregates are 0–4.75 mm natural sand with an apparent density of 2.655 g/cm<sup>3</sup>, a fineness modulus of 2.3, and a sand mud content of 2.9% measured by the volumetric flask method, and its sieving curve is shown in Figure 2b.

**Table 5.** Concrete mix design.

Mix No.	Cement	Sand	Big Stone	Small Stone	Water	Air-Entraining Superplasticizer		Water-Cement Ratio	Coarse Ratio
	(kg/m <sup>3</sup> )	(%)							
C1	320	615.6	790.02	646.38	128	6.4	2	0.4	0.3
C2	330	609.42	782.09	639.89	138.6	0	0	0.42	0.3
C3	330	613.38	787.17	644.05	125.4	6.6	2	0.38	0.3
C4	330	611.4	784.63	641.97	132	6.6	2	0.4	0.3
C5	330	609.42	782.09	639.89	138.6	6.6	2	0.42	0.3
C6	340	607.2	779.24	637.56	136	6.8	2	0.4	0.3
C7	330	570.64	807.05	660.31	132	6.6	2	0.4	0.28

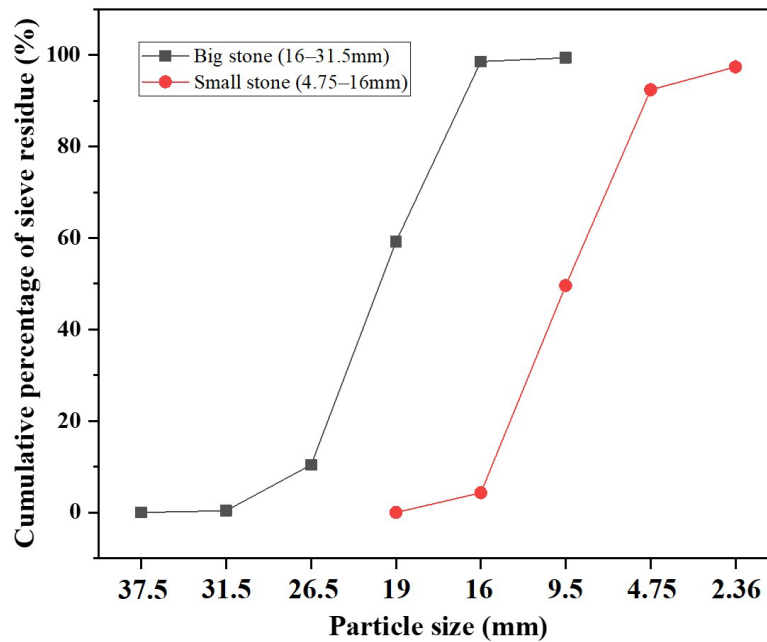
## 2.2. Test Methods

### 2.2.1. X-ray Diffraction (XRD)

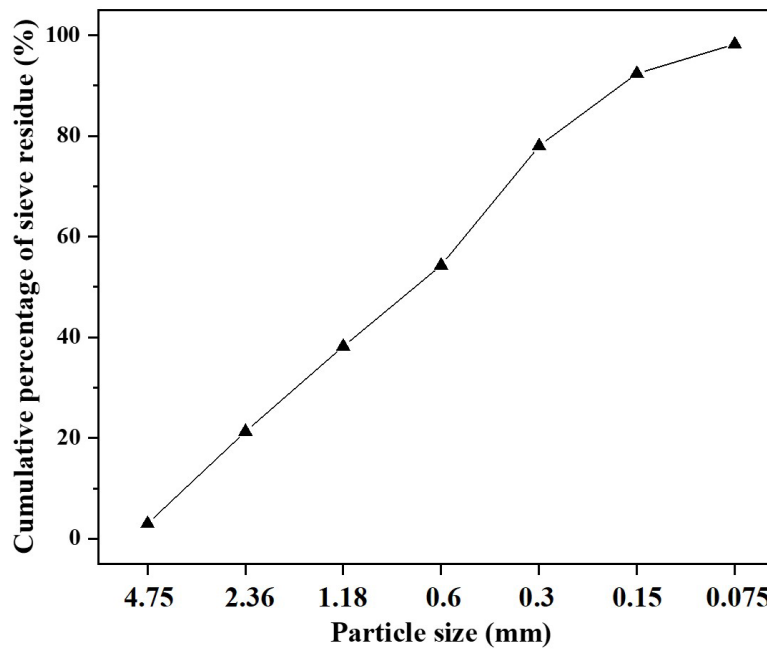
XRD patterns were collected by using a Bruker D8 powder diffractometer (Bruker, Billerica, MA, USA) with scanning angles (2θ) ranging from 5 to 70° at a rate of 0.6 s/step and 0.02°/step using a CuKα radiation source (λ = 1.5418 Å) at 40 kV and 40 mA to identify the variation in the crystalline phases. The samples were cured under standard lab environment until 28 days. All samples were ground to powder ≤ 75 μm and vacuum dried before testing.

### 2.2.2. Mechanical Testing—Compressive and Flexural Strength

The samples (150 mm × 150 mm × 550 mm) prepared following GBT 50081-2019 [31] were tested for compressive and flexural strength according to the test methods in the standard.



(a)



(b)

Figure 2. Particle size distribution of coarse aggregates (a) and fine aggregates (b).

2.2.3. Mercury Intrusion Porosimetry (MIP)

Concrete samples were broken into pieces, and the slurry fraction approximately soy-sized particles were selected and soaked in anhydrous ethanol for 24 h to terminate hydration and then placed in a vacuum drying oven at 40 °C for 3 days. After the samples were processed, the pore structure was tested using an Autopore IV9510 mercury intruder (Micromeritics Instrument Corp., Norcross, GA, USA). Samples of 3–5 g were taken for each test, with pressures ranging from 0.0036 to 414 MPa, corresponding to a minimum pore size of approximately 3 nm.

#### 2.2.4. Scanning Electron Microscopy (SEM)

After crushing, samples with a fresh broken surface were selected for SEM observations. As the sample itself is not conductive, it was coated with carbon. SEM testing is carried out using a field emission environmental scanning microscope FEI QUANTA 200 FEG (FEI, Hillsboro, OR, USA) under high vacuum at a voltage 15.0 kV to observe the microscopic morphology of the specimen. Different phases such as calcium hydroxide, CSH, and ettringite were identified with the aid of energy dispersive spectroscopy (EDS).

#### 2.2.5. Freeze-Thaw Tests

A rapid freezing method in GB 50082-2009 [32] was applied for concrete surface frost damage test. The specimen size is 100 mm × 100 mm × 400 mm. After 24 days, the specimens were removed from the maintenance room and then immersed in water at  $20 \pm 2$  °C, the surface of the water being 20–30 mm above the top surface of the specimens. After 4 days of immersion in water, the specimens were removed at age 28 days, cleaned with a damp cloth to remove the surface water, and the external dimensions were measured. The freeze-thaw cycle system is shown in Figure 3.

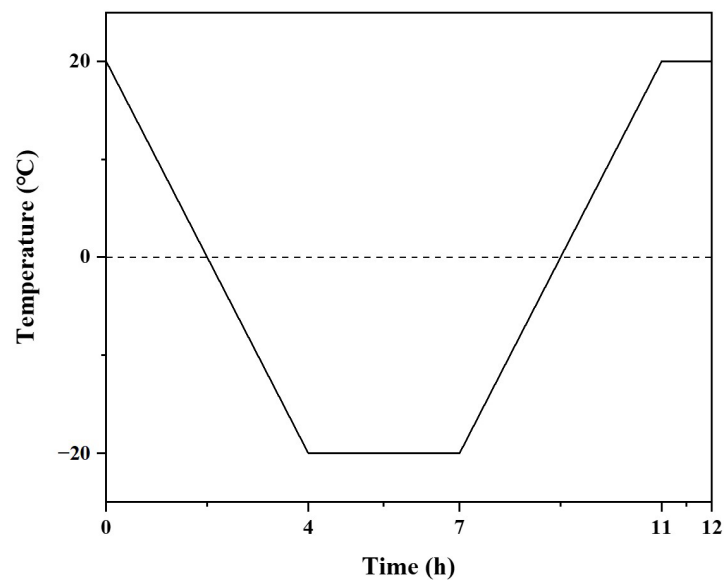


**Figure 3.** Freeze-thaw cycle system.

The relative dynamic modulus of elasticity has been calculated using the following formula:

$$P_i = \frac{f_{ni}^2}{f_{0i}^2} \times 100 \quad (1)$$

where  $P_i$  is the relative dynamic modulus of elasticity (%) of the  $i$ -th concrete specimen after  $N$  freeze-thaw cycles, with accuracy of 0.1;  $f_{ni}^2$  is first natural frequency of transverse vibrations (Hz) of the  $i$ -th concrete specimen after  $N$  freeze-thaw cycles; and  $f_{0i}^2$  is first natural frequency of transverse vibrations (Hz) of the  $i$ -th concrete specimen before the freeze-thaw cycle.

The relative dynamic modulus of elasticity is determined as the arithmetic mean of the test results of three specimens.

The mass loss rate of individual specimens has been calculated using the following formula:

$$\Delta W_{ni} = \frac{W_{0i} - W_{ni}}{W_{0i}} \times 100 \quad (2)$$

where  $\Delta W_{ni}$  is mass loss of the  $i$ -th concrete specimen after  $N$  freeze-thaw cycles (%), with accuracy of 0.01;  $W_{0i}$  is mass of the  $i$ -th concrete specimen before the freeze-thaw cycle test (g); and  $W_{ni}$  is mass of the  $i$ -th concrete specimen after  $N$  freeze-thaw cycles (g).

The average mass loss rate for each group of specimens has been determined as the arithmetic means of the three specimens' mass loss rate test results. The test frequencies are after 25, 175, 200, 225, 250, 275, and 300 cycles.

#### 2.2.6. Salt-Freezing Tests

The salt-freezing test was performed conforming to MH 5006-2015 [30] and a single-sided salt-freezing method was adopted. The specimen size was  $\varphi 150 \text{ mm} \times 100 \text{ mm}$ . Epoxy resin was coated to all sides of the test piece except for the exposure surface. The salt solution was prepared with 97% distilled water and 3% ethylene glycol. The cyclic temperature changes started at  $20 \text{ }^\circ\text{C}$  and decreased at a constant rate of  $10 \text{ }^\circ\text{C/h} \pm 1 \text{ }^\circ\text{C/h}$  to  $-20 \text{ }^\circ\text{C} \pm 1 \text{ }^\circ\text{C}$  and maintained for 3 h; then it started at  $-20 \text{ }^\circ\text{C}$  and increased at a constant rate of  $10 \text{ }^\circ\text{C/h} \pm 1 \text{ }^\circ\text{C/h}$  to  $20 \text{ }^\circ\text{C} \pm 1 \text{ }^\circ\text{C}$  and maintained for 1 h. When testing specimen spalling, samples were removed from the test chamber and placed in the ultrasonic bath with the specimen test side down for 3 min. The spalling material was collected and dropped during the ultrasonic test and filtered through filter paper. The filtered filter papers with all the exfoliated materials were dried in an oven at  $110 \text{ }^\circ\text{C} \pm 5 \text{ }^\circ\text{C}$  for 24 h and cooled in a laboratory at a temperature of  $20 \text{ }^\circ\text{C} \pm 2 \text{ }^\circ\text{C}$  and a relative humidity of  $60\% \pm 5\%$  for  $60 \text{ min} \pm 5 \text{ min}$ .

The mass of spalled material on the surface of the specimen has been calculated using the following formula:

$$m_s = m_2 - m_1 \quad (3)$$

where  $m_s$  is mass of specimen surface flake (g), with accuracy of 0.01 g;  $m_1$  is mass of filter paper (g), with accuracy of 0.01 g; and  $m_2$  is total mass of filter paper and specimen flakes after drying (g), with accuracy of 0.01 g.

The amount of spalling per unit test area for each group of specimens has been the arithmetic mean of the calculated values for three specimens.

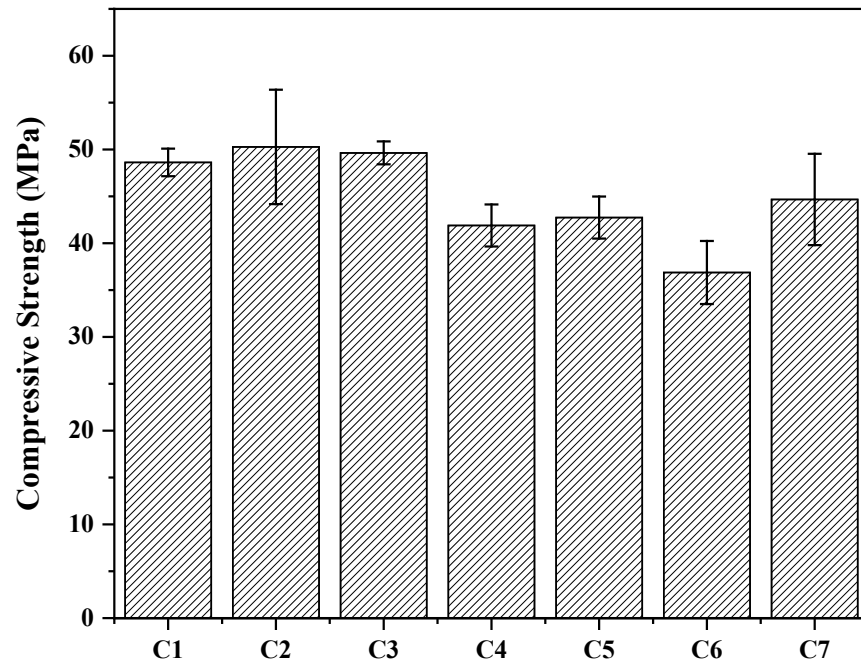
### 3. Analysis of Results

#### 3.1. Mechanical Testing Results—Compression and Flexural Testing

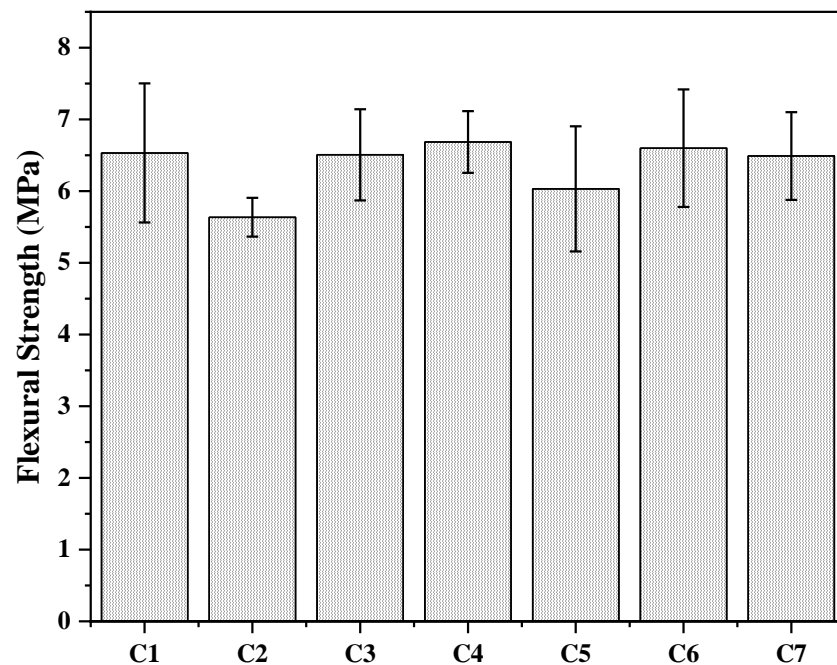
The results of the 28-day compressive and flexural strength tests for all specimens are shown in Figure 4. The C2 sample had no air-entraining superplasticizer added, and it was the control group for other mixes when considering the effect of air-entraining superplasticizer. The experimental results show that the air-entraining superplasticizer can reduce the 28-day compressive strength of concrete slightly but can improve the 28 day-flexural strength. The C3, C4, and C5 samples were compared to see the effect of the water-cement ratio, and the three groups of specimens had water-cement ratios of 0.38, 0.40, and 0.42, respectively. When the water-cement ratio increased from 0.38 to 0.40, the compressive strength of concrete decreased significantly, and the flexural strength increased slightly; when the water-cement ratio increased from 0.40 to 0.42, the compressive strength of concrete increased slightly, and the flexural strength decreased significantly.

The effect of the sand-aggregate ratio on the mechanical properties of concrete can be obtained from the comparison between the C4 and C7 samples. It can be seen that an appropriate reduction in sand-aggregate ratio, from 0.3 to 0.28, can effectively increase the compressive strength of concrete. Similar findings have been reported in the literature [21]; however, the flexural strength decreased with decreasing sand-aggregate ratio. With the increasing amount of cement in the C1, C4, and C6 samples from  $320 \text{ kg/m}^3$  to  $340 \text{ kg/m}^3$ , it is clear from the graph that the compressive strength of the concrete decreases continuously with the increasing amount of cement. However, the flexural strength does not change significantly. It is known that microcracks usually propagate from the ITZs (interfacial transition zones) in normal concrete and develop through the cement paste; then, an optimum content of cement is required because too little cement content could not generate

compacted ITZs and too much cement could increase weak points in cement paste for crack developing. In addition, cement is more expensive than other raw materials such as stone and sand. The minimum cement amount should be used when similar physical properties can be obtained.



(a)



(b)

Figure 4. Mechanical results: (a) compressive and (b) flexural strength.

### 3.2. XRD Results

The XRD results for all seven mix groups from this test are shown below in Figure 5. The C2 and C5 samples are the control groups with and without the addition of superplas-

ticizer; the C3, C4, and C5 samples have increased water-cement ratios from 0.38 to 0.42; and the C4 and C7 samples compare the change in sand-aggregate ratio. It can be seen that the addition of the superplasticizer and higher water-cement ratios induced more obvious peaks of the portlandite and ettringite due to the fact that more cement participated in the hydration. The quartz came from the sand and calcite mainly came from the stone in concrete when preparing the powder samples. Then, the main difference on the resistance of salt freezing caused by these different mixes should be discussed in more detail from the microstructure and pore distributions.

\*-Quartz [SiO<sub>2</sub>] ×-Ettringite [AFt] ◆-Portlandite [Ca(OH)<sub>2</sub>] +-Calcite [CaCO<sub>3</sub>]

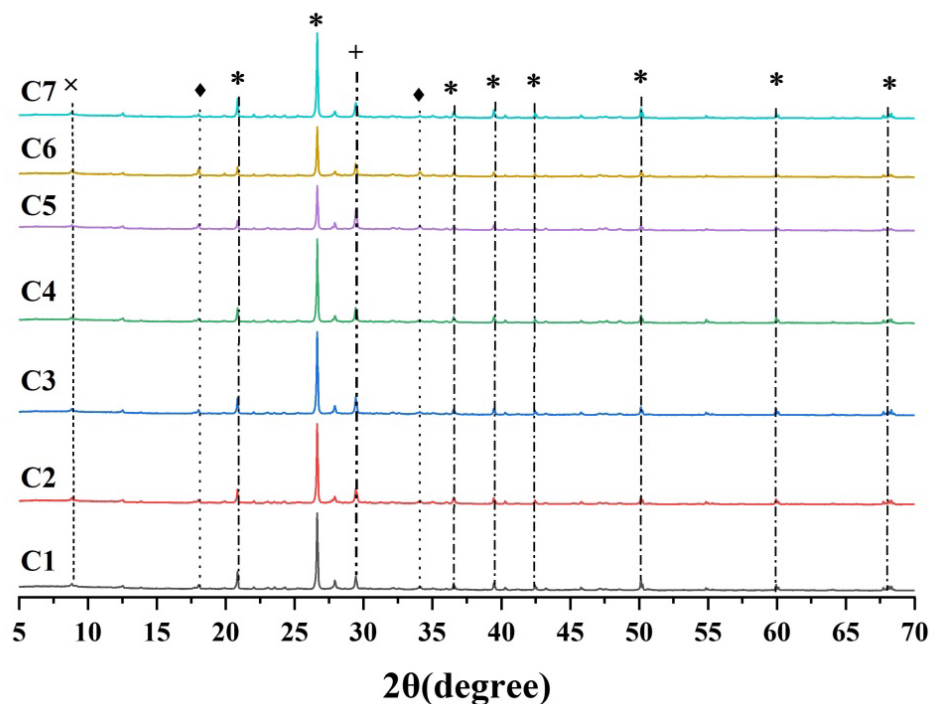


**Figure 5.** XRD results of different specimens.

### 3.3. Results of Pore Distribution in Different Mixes

Figures 6–8 show pore size distribution and porosity from MIP results of different mixes. It is well known that pore structure in concrete significantly affects the frost resistance of the concrete. When water freezes and becomes ice in concrete under cold conditions, its nucleation and growth are very rapid and can lead to a significant volume expansion [33,34]. Previous research has shown that with increasing freeze-thawing cycles, the porosity of concrete increased, and the pores became concentrated in large pores, which to a certain extent destroyed the internal structure causing microcracks [35]. Therefore, it is essential to characterize the pore structure of concrete.

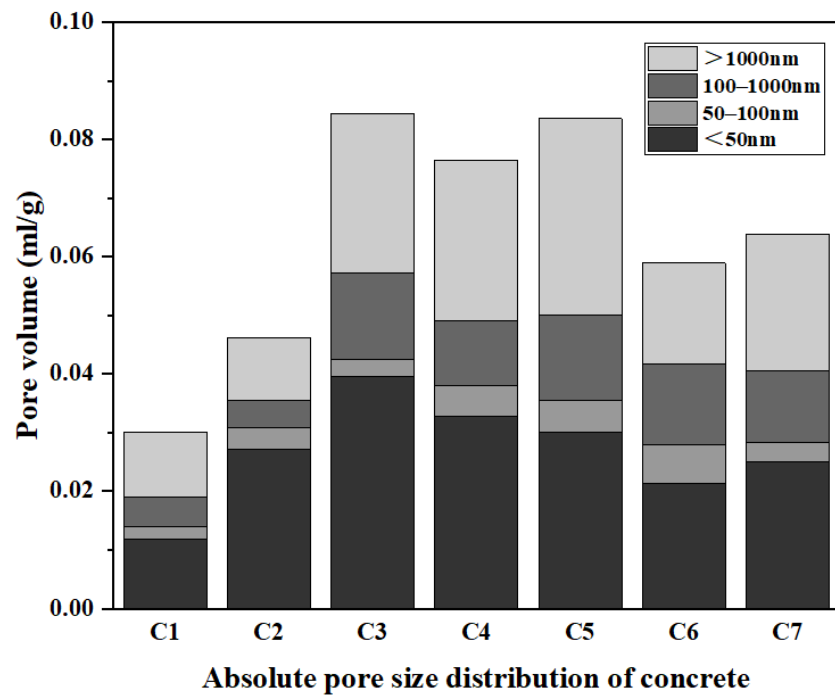


Figure 6. Size distribution of pore groups in concrete.

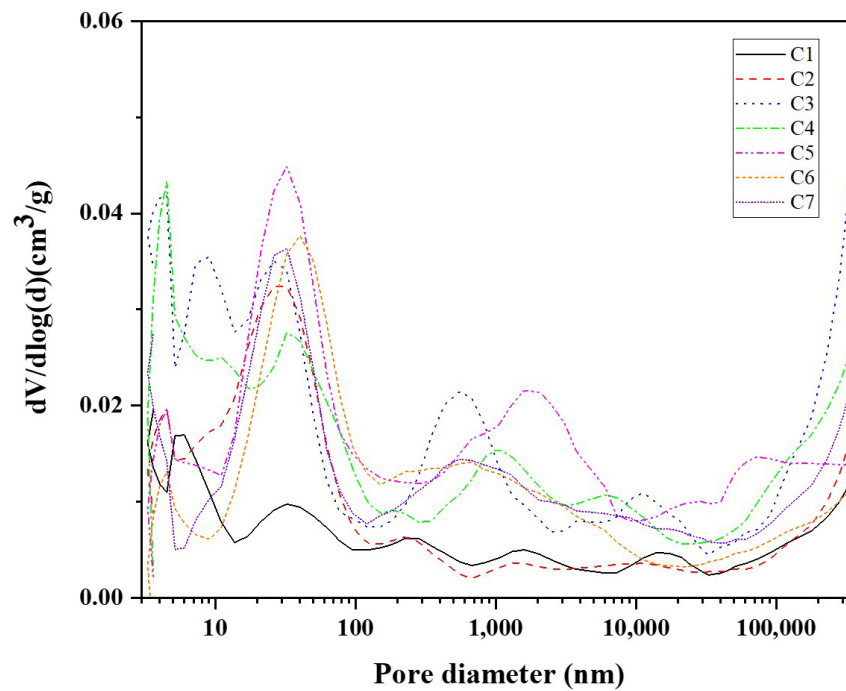
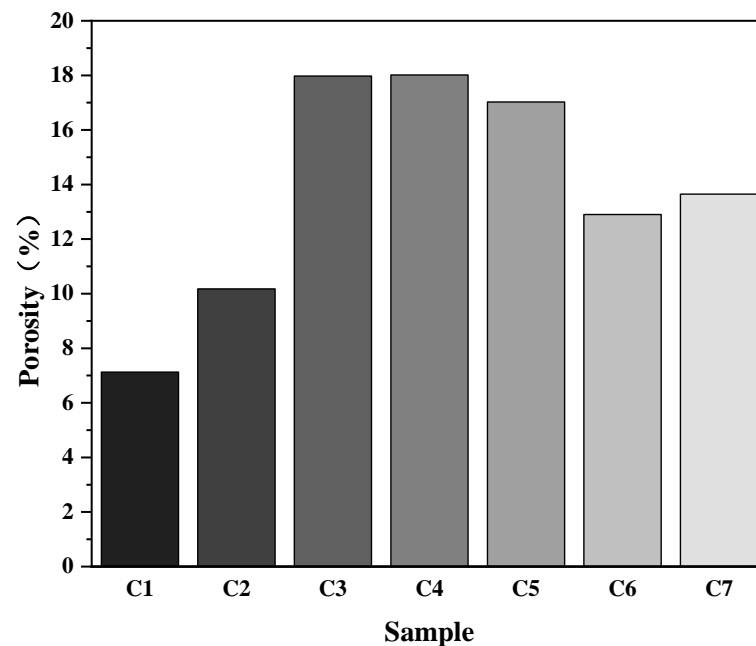


Figure 7. Pore size distribution in concrete.



**Figure 8.** Porosity of each mix group.

Figures 6 and 7 show that by comparing the results of the C2 and C5 samples, the addition of the air-entraining superplasticizer has resulted in a significant increase in the total pore content of the concrete, especially the absolute pore volume in the 100–1000 nm and >1000 nm, occupying a total of over 50%. The superplasticizer added in this study is also air-entraining. Air-entraining agents can introduce uniform, stable, and tiny bubbles in the concrete; these bubbles can effectively cushion the various stresses generated in the cement paste, playing a “buffer airbag” role, and can effectively improve the salt and frost resistance of concrete.

The results also show that with the increase in the water-cement ratio, the absolute pore volume in the <50 nm region decreases relatively, and the absolute pore volume in the 50–100 nm and >1000 nm regions show an increasing trend. An appropriate increase in the cement content and sand-aggregate ratio can help to increase the total pore content of the concrete as well as the absolute pore volumes in all four zones, as shown in Figures 6 and 7. It should be kept in mind that porosity also affects the strength of concrete [36–40]. In Figure 8, the porosity of the C3, C4, and C5 samples are similar, but in Figure 4, the compressive strength of the C4 sample is significantly lower than the C3 samples, and the flexural strength of the C3 and C4 samples are higher than the C5 samples. It can be seen that the relationship between porosity and compressive and flexural strength interactions is not direct and could be quite complicated, which could involve the microstructure and the connectivity of micropores.

### 3.4. Microstructure Observations

Figure 9 shows the microscopic morphology of the C1–C7 samples. It can be seen that the ITZ in added air-entraining superplasticizer mix (the C5 sample) is slightly different from the mix with no air-entraining superplasticizer (the C2 sample), and the addition of the superplasticizer resulted in a more compact bond between aggregate and cement matrix in the concrete. Compared to the C2 sample, the micro pores in the C5 sample are more evenly distributed and the pore sizes in the paste of the C5 sample are similar. In the C3, C4, and C5 samples, with the water-cement ratio slightly changing from 0.38 to 0.40 and 0.42, there is no obvious difference in the microstructure in these 3 mixes, which agrees well with the MIP results. In the C6 and C7 samples, the effect of the sand-aggregate ratio on the microstructure cannot be seen from the SEM images. Comparing the C1 and C6 samples, the effect of cement content on the microstructure is also not obvious, but the C1

sample has less cement paste and then fewer pores as reported in MIP results compared with the C6 sample.

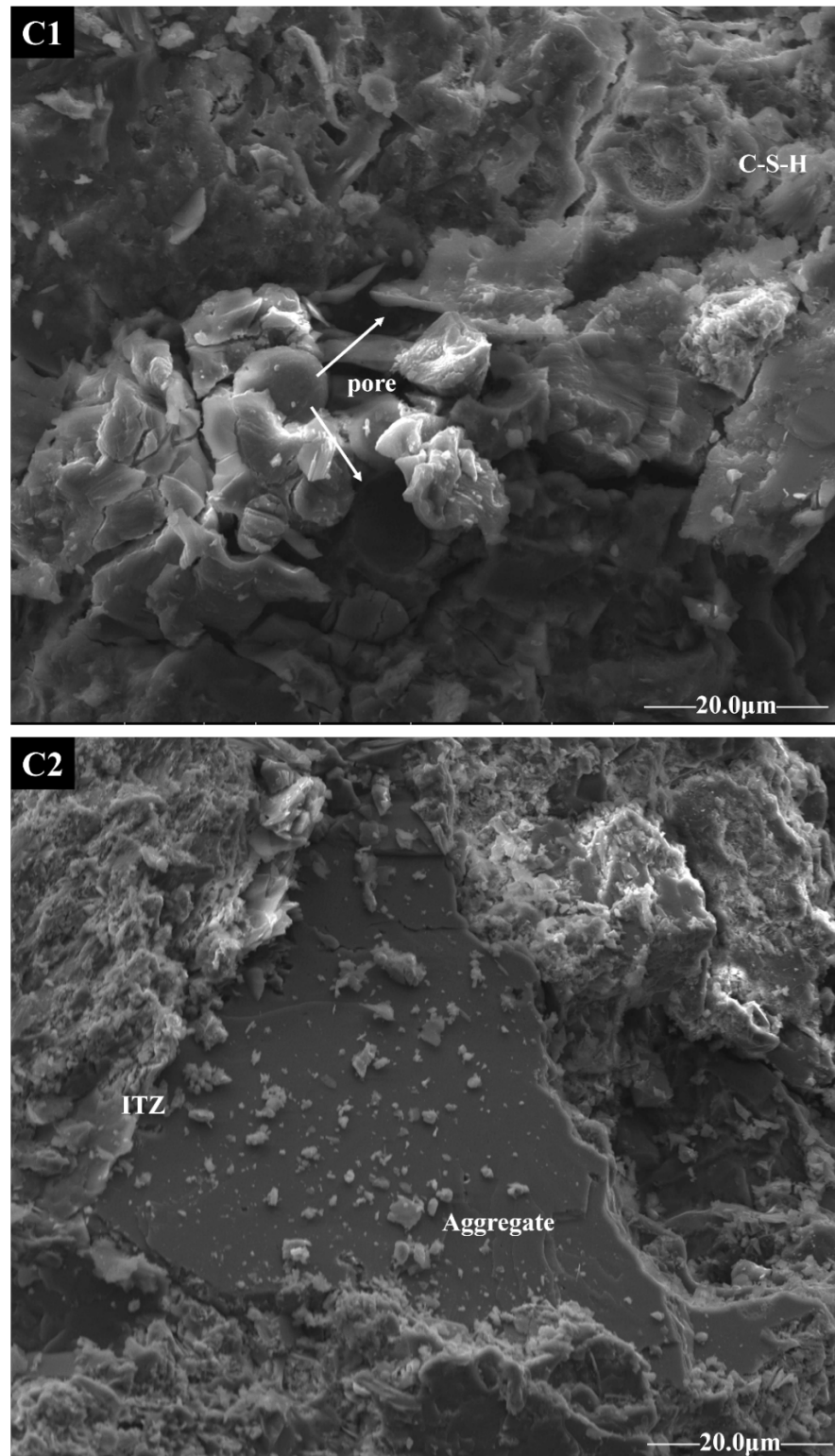


Figure 9. Cont.

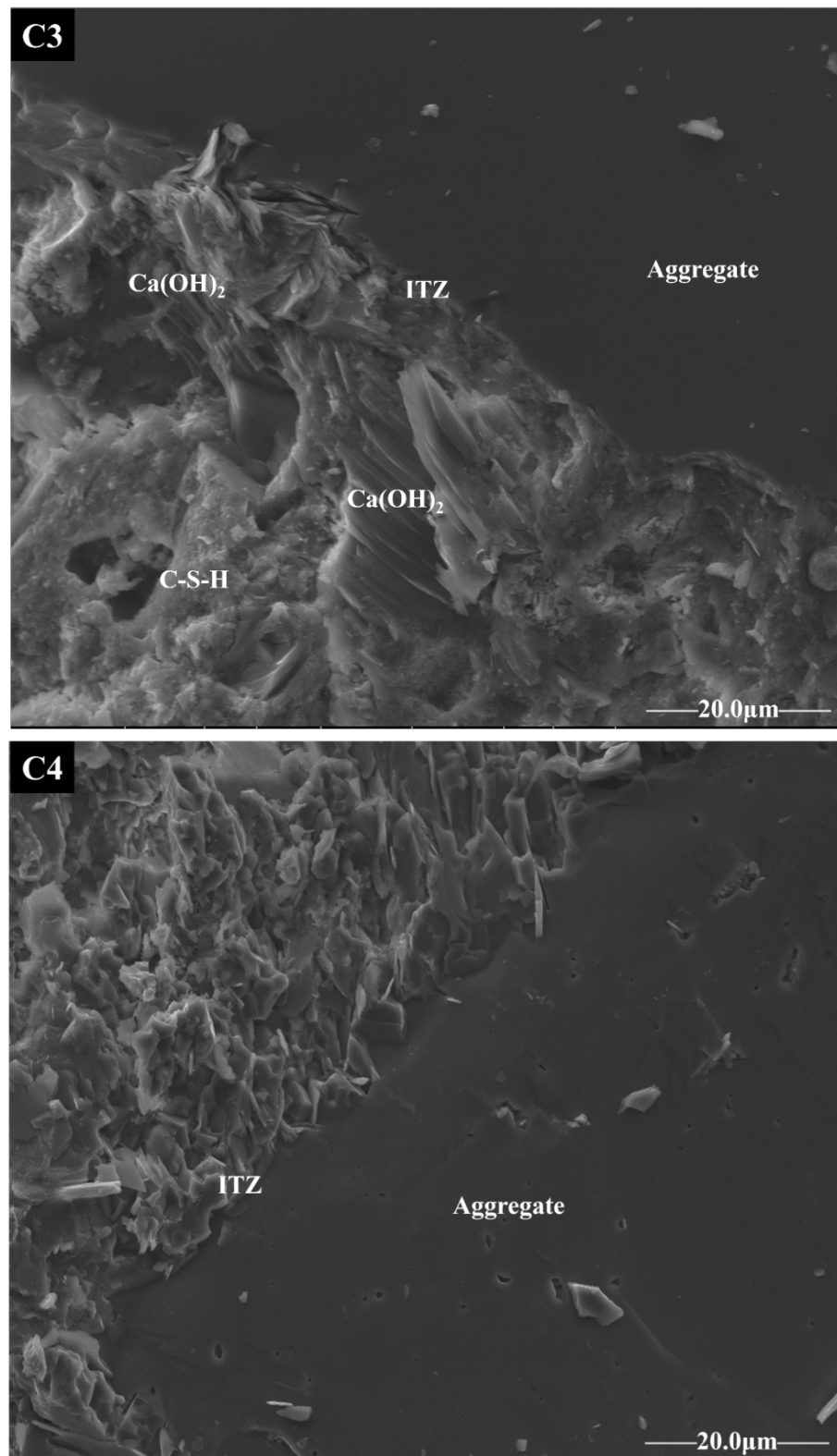


Figure 9. Cont.

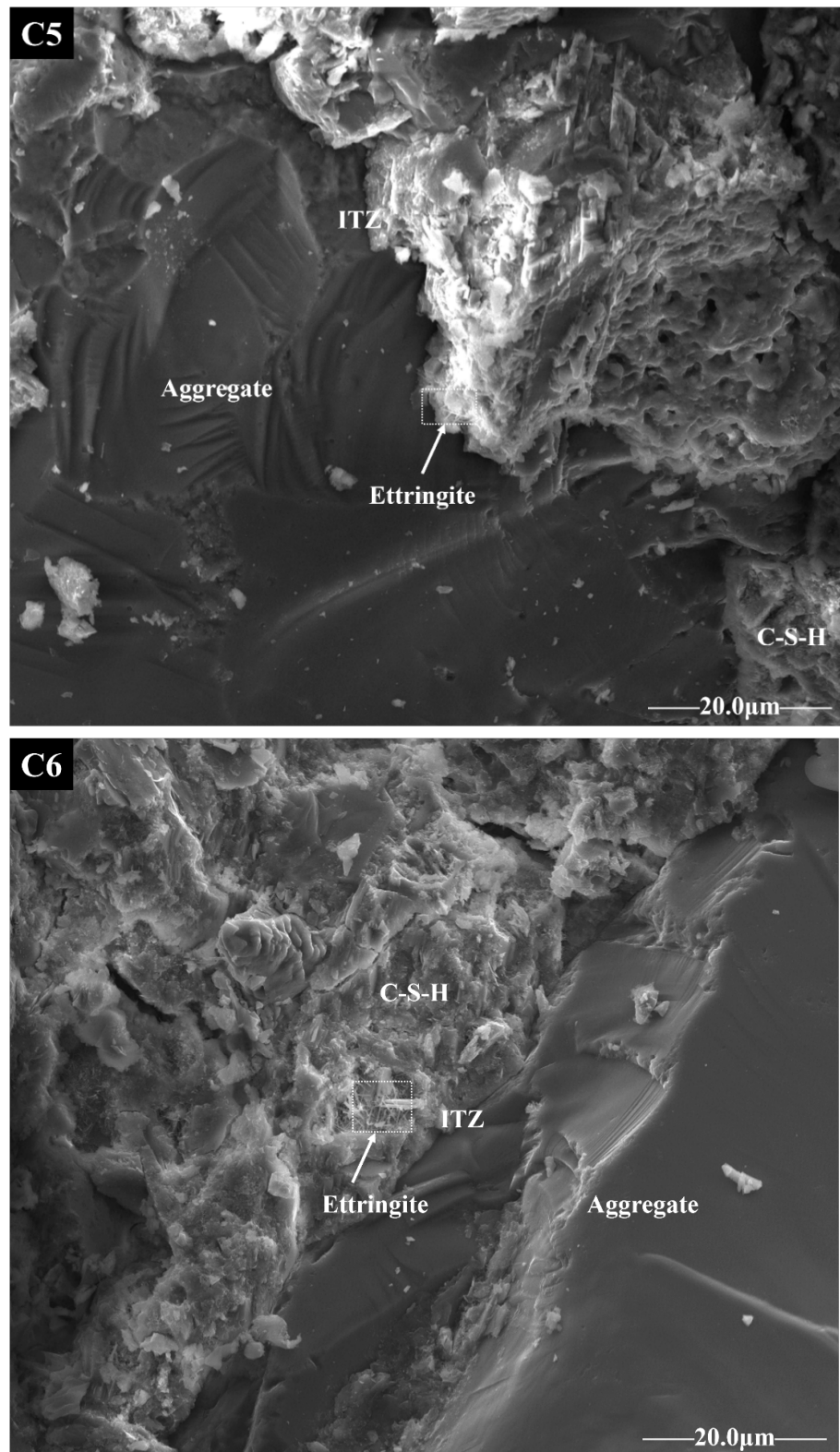


Figure 9. Cont.

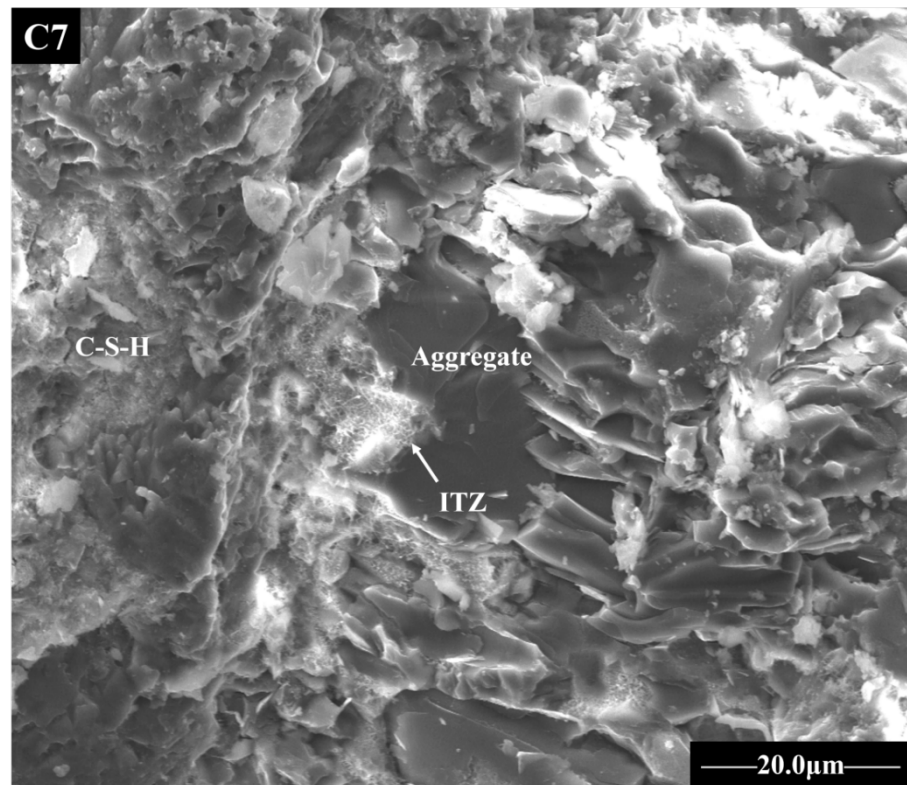
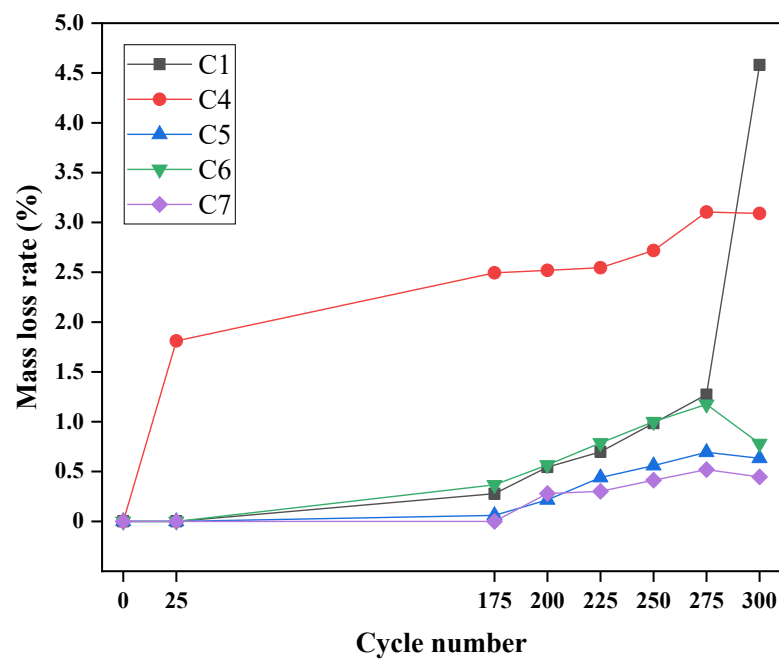


Figure 9. Micromorphology results observed by SEM.

3.5. Physical Performance of Different Mixes Subjected to Freeze-Thawing Cycles

Based on the analysis of the above experiments, the C1, C4, C5, C6, and C7 samples specimens were selected for further freeze-thawing experiments. The mass loss rate and relative dynamic modulus of elasticity during test cycles are shown in Figure 10.



(a)

Figure 10. Cont.

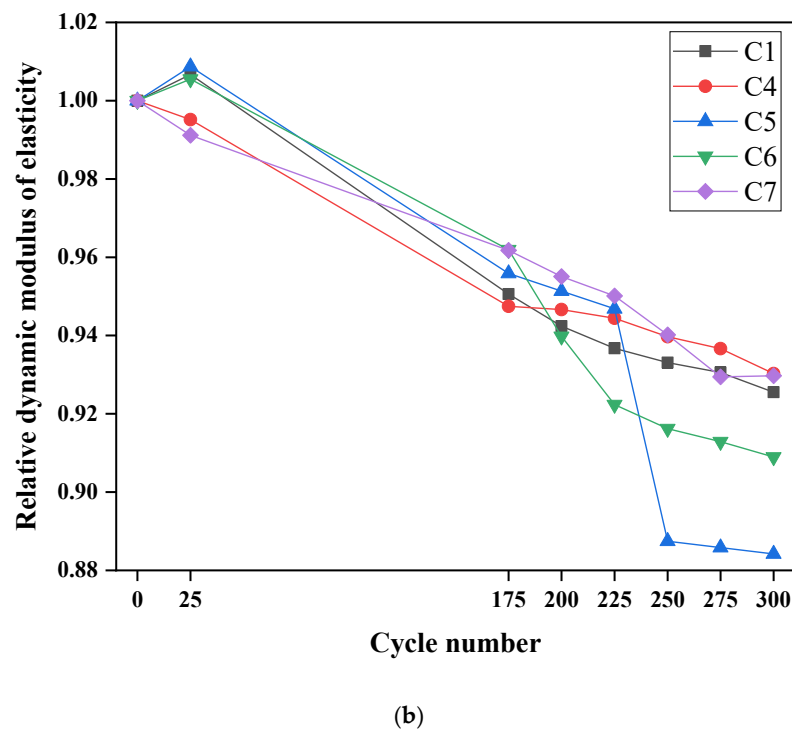


**Figure 10.** Results of mass loss (a) and relative dynamic modulus of elasticity (b) after freeze-thawing tests.

In Figure 10a, for the C1, C4, and C6 samples, the amount of cement increased from  $320 \text{ kg/m}^3$  to  $340 \text{ kg/m}^3$ , and the mass loss rate of the C1 sample decreased significantly after 275 freeze-thawing cycles. Additionally, the C4 sample had consistently higher mass loss rates than the other groups after the start of the freeze-thawing cycles. The C6 sample showed a significant increase in mass loss rate at 25–175 freeze-thawing cycles compared to the C7 sample, which could be caused by the different sand-aggregate ratios. However, since the difference in sand-aggregate ratios is relatively small, there could be other factors, such as the pore structure.

The change of relative dynamic modulus of elasticity for all mixes after different freeze-thawing cycles is shown in Figure 10b. From Figure 10a, the C1 sample showed a significant decrease in mass loss after 275 freeze-thawing cycles; however, in Figure 10b, there was no responding change of the dynamic modulus of elasticity in the same test cycles. It can be seen that there is no direct relationship between the mass loss and the change of dynamic modulus of concrete subjected to freeze-thawing.

### 3.6. Effects of Different Surface Treatments on the Physical Performance of Concrete Subjected to Salt-Freezing Cycles

By considering the mechanical properties and freeze-thawing performance from the above experimental results, the C4 sample specimens were selected for further salt-freezing experiments. A total of 4 different treatments shown in Figure 11 were considered, and the concrete specimens were subjected to 30 salt-freezing tests. Additionally, the total scaling mass per unit area in 10, 20, and 30 salt-freezing cycles are shown in Figure 12. In these surface treatment methods, smoothing means that the surface of the formed specimen is smoothed, brushing means that the surface of the formed specimen is brushed according to the requirements of the airport road surface brushing, impregnation means that the exposed surface of the concrete specimen had been soaked with silane in a depth of 5 mm for one day, and spraying means that the exposed surface of the concrete specimen is sprayed with 300 g of silane per square meter. Brushing is usually mandatory for airport

pavement roads to increase the friction coefficient to ensure the safety of aircraft landing and take-off.



**Figure 11.** (a) Smoothing; (b) brushing; (c) brushing + spraying silane; and (d) brushing + silane-impregnated.

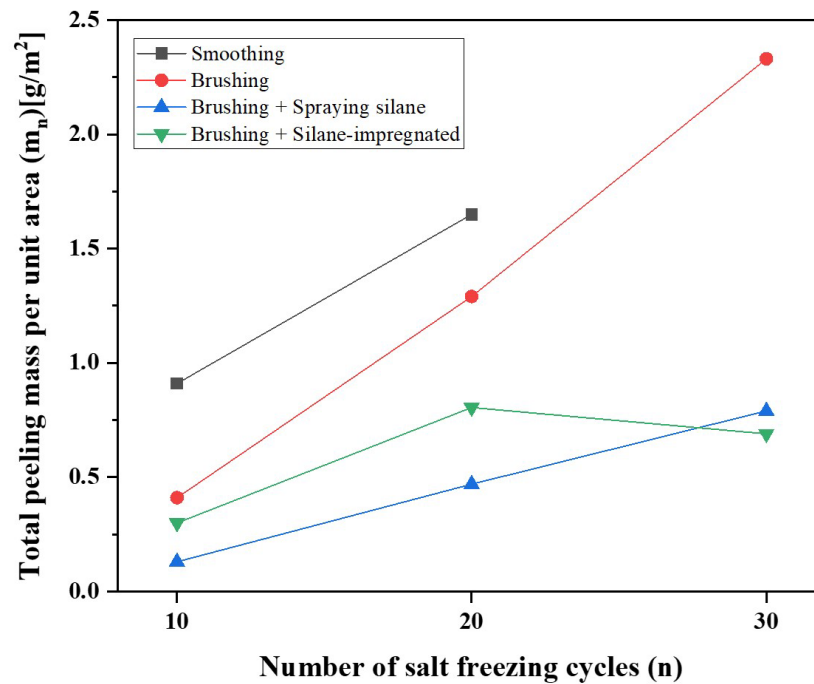


**Figure 12.** Total scaling mass per unit area in 10, 20, and 30 salt-freezing cycles.

The results show that specimens only smoothed and brushed had a higher spalled mass loss in the salt-freezing tests than the other two groups, namely brushing + spraying silane and brushing + silane impregnated. In particular, the spalled mass of the brushed specimens tended to increase continuously with increasing salt-freezing test cycles. The specimens sprayed with silane or impregnated with silane had a significantly lower spalled mass than the no silane-treated specimen group after 30 cycles of salt-freezing tests. The spalling quality of the specimens with spraying silane is lower than that with silane impregnated, and it can be inferred that silane impregnation is conducive to improving the frost resistance of concrete and, to a certain extent, the durability of concrete. The chemical reactions can occur between silane and hydration products on the concrete surfaces, forming a network structure of dimer or even polymer on the concrete surface. From this salt-freezing experiment, the spraying silane method could provide a better protection mechanism than the impregnating silane method. Brushing and spraying silane reduced the mass loss by more than 60%.

#### 4. Discussion

##### 4.1. Change of Airport Pavement Concrete in High Plateau Subjected to Freeze-Thawing and Salt Freezing

Airport pavement concrete on a high plateau is susceptible to freeze-thawing and salt-freezing damage due to the located environment. During freeze-thawing cycles, the concrete is damaged, mainly in terms of reduction in dynamic modulus of elasticity and loss of quality due to surface spalling [41]. From the viewpoint of mechanical properties, it is mainly manifested as the reduction in mechanical property indexes such as compressive strength, flexural strength, and static modulus of elasticity. Moreover, from the microscopic viewpoint, it is manifested as the expansion of micro-cracks and the degradation of the matrix in concrete [42–46] from dense to loose. The dynamic modulus of elasticity of concrete and transport properties [47,48] is closely related to the structure of the concrete itself, and when the internal structure of the concrete changes, the dynamic modulus of elasticity changes at the same time [49].

#### *4.2. Effect of Water-Cement Ratio and Cement Amount on the Frost Resistance of Airport Pavement Concrete*

Concrete with a high water-cement ratio usually has poor frost resistance [50]. In this research, the results show that a slight change in the water-cement ratio had no significant effect on the surface spalling of concrete in freeze-thawing cycles, but it reduced the dynamic modulus of elasticity, especially after 225–250 freeze-thawing cycles. The slight change in cement amount was found to have no significant effect on the rate of loss of mass spalled at 25–275 freeze-thawing cycles, but the use of more cement caused a significant decrease in the dynamic modulus of elasticity of the concrete after 175 freeze-thawing cycles.

#### *4.3. Effect of Different Surface Treatments on Salt-Freezing Resistance*

The physical treatment of concrete surfaces with brushing alone cannot effectively resist the damage caused by salt frost. A brushed concrete surface followed by a silane surface treatment can significantly improve the resistance of concrete to salt freezing. Spraying silane as well as silane impregnation on the surface of the concrete material alone will improve the resistance of the material to salt freezing, with spraying silane having better performance and easier operation. It is important to note that the water repellency created by silane impregnation of the surface could decay over time [26]. The long-term effects of silane-impregnated and silane-sprayed surface treatments still require extensive experimental research on airport concrete pavements.

#### *4.4. Important Physical Properties for Airport Pavement Concrete in High Plateau*

The results from this study show that C4 specimens (water-cement ratio = 0.4, 2% naphthalene air-entraining superplasticizer and sand-aggregate ratio = 0.3), with brushing and silane spraying on the surface, are more resistant to freeze-thawing and salt-freezing damage. Han et al. [51] conducted salt-freezing experiments by preparing hardened mortars with different water-cement ratios and concluded that cement mortars with a less water-cement ratio have a stronger frost resistance. Other methods, such as additives [52], pre-treatments [53], and surface treatments [54], are suggested to compare them with silane impregnation in order to achieve a better frost resistance of concrete.

### **5. Conclusions**

This paper investigates the effects of combined air-entraining superplasticizer and surface treatments of airport pavement concrete against salt freezing, and related mechanisms were analyzed. Based on the results, the following conclusions can be drawn:

- (1) The addition of an air-entraining superplasticizer can modify the ITZ, increase bonding between aggregates and cement matrix, and substantially increase the porosity of concrete. However, it has an adverse effect on the compressive strength properties of the concrete due to the increased porosity, but this effect is not significant to the flexural strength properties of the concrete. Therefore, the optimum amount of air-entraining superplasticizer should be added in order to increase the porosity of airport pavement concrete on high plateau without compromising the compressive and flexural strength of concrete. In addition, using air-entraining superplasticizer only might not be able to provide a proper freezing resistance to airport pavement, and proper surface treatments could be applied.
- (2) Both silane spraying and silane impregnation methods effectively improved the salt-freezing resistance of concrete, with silane spraying more effective. Silane spraying and impregnation make the concrete from the surface to the ingress depth water-repellent, but the long-term performance of silane spraying and impregnation still needs further experimental work. Surface treatment by brushing and silane reduced the mass loss by more than 60% in the salt-freezing tests.
- (3) Freeze-thawing in concrete caused microcracks to expand and develop, and the C-S-H gel structure becomes loosened within the concrete. In order to have a better freezing

resistance, promoting cement early hydration process, combined modification of the microstructure by air-entraining superplasticizer, and silane spraying are suggested to improve the salt-freezing resistance of concrete.

**Author Contributions:** Conceptualization, J.W.; methodology, M.L., Y.L. (Yong Lai), D.M., J.W., L.X., L.L., Z.G. and Y.L. (Yan Liu); software, J.W.; validation, J.W.; formal analysis, M.L., Y.L. (Yong Lai), D.M., J.W., L.X., L.L., Z.G., Y.L. (Yan Liu), Y.G., L.Z. and Y.Z.; investigation, M.L., Y.L. (Yong Lai), D.M. and L.X.; resources, J.W.; data curation, M.L., Y.L. (Yong Lai), D.M., J.W. and L.X.; writing—original draft, M.L., J.W., L.L., Z.G. and Y.L. (Yan Liu); writing—review & editing, M.L., J.W., L.L., Z.G., Y.L. (Yan Liu), Y.G., L.Z. and Y.Z.; visualization, M.L., Y.L. (Yong Lai), D.M., L.X., L.L. and Z.G.; supervision, J.W.; project administration, J.W.; funding acquisition, J.W. All authors have read and agreed to the published version of the manuscript.

**Funding:** This research was funded by the National Natural Science Foundation of China (Nos. 52008232 and 52038004).

**Institutional Review Board Statement:** Not applicable.

**Informed Consent Statement:** Not applicable.

**Data Availability Statement:** The data presented in this study are available on request from the corresponding author.

**Acknowledgments:** The authors wish to acknowledge the support provided from Beijing Super-Creative Technology Co., Ltd.

**Conflicts of Interest:** The authors declare no conflict of interest.

## References

1. Wang, L.; Guo, F.X.; Yang, H.M.; Wang, Y.; Tang, S.W. Comparison of FLY ASH, PVA fiber, MgO and shrinkage-reducing admixture on the frost resistance of face slab concrete via pore structural and fractal analysis. *Fractals* **2021**, *29*, 2140002. [[CrossRef](#)]
2. Prakash, R.; Divyah, N.; Srividhya, S.; Avudaiappan, S.; Amran, M.; Raman, S.N.; Guindos, P.; Vatin, N.I.; Fediuk, R. Effect of steel fiber on the strength and flexural characteristics of coconut shell concrete partially blended with fly ash. *Materials* **2022**, *15*, 4272. [[CrossRef](#)] [[PubMed](#)]
3. Divyah, N.; Prakash, R.; Srividhya, S.; Sivakumar, A. Parametric study on lightweight concrete-encased short columns under axial compression-comparison of design codes. *Struct. Eng. Mech.* **2022**, *83*, 387–400.
4. Sundaresan, S.; Ramamurthy, V.; Meyappan, N. Improving mechanical and durability properties of hypo sludge concrete with basalt fibres and SBR latex. *Adv. Concr. Constr.* **2021**, *12*, 327–337.
5. Huo, J.; Wang, Z.; Chen, H.; He, R. Impacts of low atmospheric pressure on properties of cement concrete in plateau areas: A literature review. *Materials* **2019**, *12*, 1384. [[CrossRef](#)]
6. Lin, H.; Han, Y.; Liang, S.; Gong, F.; Han, S.; Shi, C.; Feng, P. Effects of low temperatures and cryogenic freeze-thaw cycles on concrete mechanical properties: A literature review. *Constr. Build. Mater.* **2022**, *345*, 128287. [[CrossRef](#)]
7. Wu, K.; Han, H.; Xu, L.; Gao, Y.; Yang, Z.; Jiang, Z.; Schutter, G. The improvement of freezing-thawing resistance of concrete by cellulose/polyvinyl alcohol hydrogel. *Constr. Build. Mater.* **2021**, *291*, 123274. [[CrossRef](#)]
8. Zhang, P.; Sha, D.; Li, Q.; Zhao, S.; Ling, Y. Effect of nano silica particles on impact resistance and durability of concrete containing coal fly ash. *Nanomaterials* **2021**, *11*, 1296. [[CrossRef](#)]
9. Ahin, Y.; Akkaya, Y.; Tademir, M.A. Effects of freezing conditions on the frost resistance and microstructure of concrete. *Constr. Build. Mater.* **2020**, *270*, 121458.
10. Powers, T.C. A working hypothesis for further studies of frost resistance of concrete. *J. Am. Concr. Inst.* **1945**, *16*, 245–272.
11. Powers, T.C.; Helmuth, R.A. Theory of volume changes in hardened Portland cement paste during freezing. *Highw. Res. Board Proc.* **1953**, *32*, 285–297.
12. Sun, M.; Zou, C.; Xin, D. Pore structure evolution mechanism of cement mortar containing diatomite subjected to freeze-thaw cycles by multifractal analysis. *Cem. Concr. Comp.* **2020**, *114*, 103731. [[CrossRef](#)]
13. Pigeon, M.; Marchand, J.; Pleau, R. Frost resistant concrete. *Constr. Build. Mater.* **1996**, *10*, 339–348. [[CrossRef](#)]
14. MacInnis, C.; Račić, D. The effect of superplasticizers on the entrained air-void system in concrete. *Cem. Concr. Res.* **1986**, *16*, 345–352. [[CrossRef](#)]
15. Plante, P.; Pigeon, M.; Saucier, F. Air-void stability, part II: Influence of superplasticizers and cement. *ACI Mater. J.* **1989**, *86*, 581–589.
16. Spörel, F.; Brameshuber, S.U. Investigations on the influence of fly ash on the formation and stability of artificially entrained air voids in concrete. *Mater. Struct.* **2009**, *42*, 227–240. [[CrossRef](#)]
17. Pigeon, M.; Plante, P.; Plante, M. Air void stability, Part I: Influence of silica fume and other parameters. *Mater. J.* **1989**, *86*, 482–490.

18. Wang, J.; Xie, J.; Wang, Y.; Liu, Y.; Ding, Y. Rheological properties, compressive strength, hydration products and microstructure of seawater-mixed cement pastes. *Cem. Concr. Compos.* **2020**, *114*, 103770. [[CrossRef](#)]
19. Chatterji, S. Freezing of air-entrained cement-based materials and specific actions of air-entraining agents. *Cem. Concr. Compos.* **2003**, *25*, 759–765. [[CrossRef](#)]
20. Ke, G.; Zhang, J.; Tian, B.; Wang, J. Characteristic analysis of concrete air entraining agents in different media. *Cem. Concr. Res.* **2020**, *135*, 106142. [[CrossRef](#)]
21. Gao, Y.; Gao, Y.; Shi, Q. Study on the influence of concrete strength and the amount of admixture with sand fineness and sand ratio. *Fly Ash Compr. Util.* **2014**, *3*, 3.
22. Dang, Y.; Xie, N.; Kessel, A.; McVey, E.; Pace, A.; Shi, X. Accelerated laboratory evaluation of surface treatments for protecting concrete bridge decks from salt scaling. *Constr. Build. Mater.* **2014**, *55*, 128–135. [[CrossRef](#)]
23. Pan, X.; Shi, Z.; Shi, C.; Ling, T.-C.; Li, N. A review on concrete surface treatment Part I: Types and mechanisms. *Constr. Build. Mater.* **2016**, *132*, 578–590. [[CrossRef](#)]
24. Du, Z. *Organosilicon Chemistry*; Higher Education Press: Beijing, China, 1990; pp. 184–206. (In Chinese)
25. Fowler, D.W.; De Puy, D.W.; Saud, A.B.; Fontana, J.; Pickard, S.S. Guide for the use of polymers in concrete. *ACI Commun.* **1986**, *548*, 1–9.
26. Li, K.; Jing, W.; Yang, R. Review on silane impregnation of concrete surface and its long-term hydrophobic performance. *J. Chin. Ceram. Soc.* **2019**, *47*, 10.
27. Basheer, L.; Cleland, D. Freeze-thaw resistance of concretes treated with pore liners. *Constr. Build. Mater.* **2006**, *20*, 990–998. [[CrossRef](#)]
28. GB175-2007; Common Portland Cement. China Quality Standards Publishing & Media Co., Ltd.: Beijing, China, 2007.
29. GB8076-2008; Concrete Admixtures. China Quality Standards Publishing & Media Co., Ltd.: Beijing, China, 2008.
30. MH 5006-2015; Specifications for Construction of Aerodrome Cement Concrete Pavement. Civil Aviation Administration of China: Beijing, China, 2015.
31. GBT 50081-2019; Standard for Test Methods of Concrete Physical and Mechanical Properties. China Quality Standards Publishing & Media Co., Ltd.: Beijing, China, 2019.
32. GB50082; Standard for Test Methods of Long-Term Performance and Durability of Ordinary Concrete. China Quality Standards Publishing & Media Co., Ltd.: Beijing, China, 2009.
33. Kaufmann, J.P. Experimental identification of ice formation in small concrete pores. *Cem. Concr. Res.* **2004**, *34*, 1421–1427. [[CrossRef](#)]
34. Beaudoin, J.J.; MacInnis, C. The mechanism of frost damage in hardened cement paste. *Cem. Concr. Res.* **1974**, *4*, 139–147. [[CrossRef](#)]
35. Wardeh, G.; Mohamed, M.A.; Ghorbel, E. Analysis of concrete internal deterioration due to frost action. *J. Build. Phys.* **2010**, *35*, 54–82. [[CrossRef](#)]
36. Kumar, R.; Bhattacharjee, B. Porosity, pore size distribution and in situ strength of concrete. *Cem. Concr. Res.* **2003**, *33*, 155–164. [[CrossRef](#)]
37. Das, B.; Kondraivendhan, B. Implication of pore size distribution parameters on compressive strength, permeability and hydraulic diffusivity of concrete. *Constr. Build. Mater.* **2012**, *28*, 382–386. [[CrossRef](#)]
38. Jin, S.; Zhang, J.; Han, S. Fractal analysis of relation between strength and pore structure of hardened mortar. *Constr. Build. Mater.* **2017**, *135*, 1–7. [[CrossRef](#)]
39. Lian, C.; Zhuge, Y.; Beecham, S. The relationship between porosity and strength for porous concrete. *Constr. Build. Mater.* **2011**, *25*, 4294–4298. [[CrossRef](#)]
40. Chen, X.; Wu, S.; Zhou, J. Influence of porosity on compressive and tensile strength of cement mortar. *Constr. Build. Mater.* **2013**, *40*, 869–874. [[CrossRef](#)]
41. Cho, T. Prediction of cyclic freeze-thaw damage in concrete structures based on response surface method. *Constr. Build. Mater.* **2007**, *21*, 2031–2040. [[CrossRef](#)]
42. Wang, J.; Xie, J.; He, J.; Sun, M.; Yang, J.; Li, L. Combined use of silica fume and steel fibre to improve fracture properties of recycled aggregate concrete exposed to elevated temperature. *J. Mater. Cycles Waste Manag.* **2020**, *22*, 862–877. [[CrossRef](#)]
43. Xie, J.; Zhao, J.; Wang, J.; Huang, P.; Liu, J. Investigation of the high-temperature resistance of sludge ceramsite concrete with recycled fine aggregates and GGBS and its application in hollow blocks. *J. Build. Eng.* **2020**, *34*, 101954. [[CrossRef](#)]
44. Hang, H.; Wang, Y.; Wang, J. Effects of aggregate micro fines (AMF), aluminum sulfate and polypropylene fiber (PPF) on properties of machine-made sand concrete. *Appl. Sci.* **2019**, *9*, 2250.
45. Xie, J.; Zhao, J.; Wang, J.; Fang, C.; Yuan, B.; Wu, Y. Impact behaviour of fly ash and slag-based geopolymeric concrete: The effects of recycled aggregate content, water-binder ratio and curing age. *Constr. Build. Mater.* **2022**, *331*, 127359. [[CrossRef](#)]
46. Wang, Y.; Lu, H.; Wang, J.; He, H. Effects of highly crystalized nano C-S-H particles on performances of portland cement paste and its mechanism. *Crystals* **2020**, *10*, 816. [[CrossRef](#)]
47. Wang, J.; Liu, E. The relationship between steady-state chloride diffusion and migration coefficients in cementitious materials. *Mag. Concr. Res.* **2020**, *72*, 1016–1026. [[CrossRef](#)]
48. Wang, J. Steady-state chloride diffusion coefficient and chloride migration coefficient of cracks in concrete. *J. Mater. Civ. Eng.* **2017**, *29*, 1966. [[CrossRef](#)]

49. Chatterji, S. Aspects of freezing process in porous material-water system: Part 2. Freezing and properties of frozen porous materials. *Cem. Concr. Res.* **1999**, *29*, 781–784. [[CrossRef](#)]
50. Tan, Y.; Zhou, C.; Zhong, C.; Zhou, J. Freeze-thaw and thermal cycle durability of pervious concrete with different aggregate sizes and water–cement ratios. *Int. J. Pavement Eng.* **2022**. [[CrossRef](#)]
51. Han, J.; Yan, C.; Hu, W.; Zhu, S.; Yan, S. Pores evolution and characterization of hardened cement mortar with different water/cement ratios under capillary suction of deicing solution freeze-thaw action. *J. Chin. Ceram. Soc.* **2020**, *48*, 10.
52. Wang, J.; Liu, E. Upcycling waste seashells with cement: Rheology and early-age properties of Portland cement paste. *Resour. Conserv. Recycl.* **2020**, *155*, 104680. [[CrossRef](#)]
53. Wang, J.; Xu, L.; Li, M.; He, H.; Wang, Y.; Xiang, D.; Lin, S.; Zhong, Y.; Zhao, H. Effect of pre-carbonation on the properties of ce-ment paste subjected to high temperatures. *J. Build. Eng.* **2022**, *51*, 104337. [[CrossRef](#)]
54. Mu, M.; Ou, C.-Y.; Wang, J.; Liu, Y. Surface modification of prototypes in fused filament fabrication using chemical vapour smoothing. *Addit. Manuf.* **2020**, *31*, 100972. [[CrossRef](#)]

**Disclaimer/Publisher’s Note:** The statements, opinions and data contained in all publications are solely those of the individual author(s) and contributor(s) and not of MDPI and/or the editor(s). MDPI and/or the editor(s) disclaim responsibility for any injury to people or property resulting from any ideas, methods, instructions or products referred to in the content.